Temperature dependent scintillation properties of pure $LaCl_3$

2009 J. Phys.: Condens. Matter 21 235605

(http://iopscience.iop.org/0953-8984/21/23/235605)

J. Phys.: Condens. Matter **21** (2009) 235605 (7pp) doi:10.1088/0953-8984/21/23/235605

Temperature dependent scintillation properties of pure $LaCl_3$

G Bizarri and P Dorenbos

Faculty of Applied Sciences, Delft University of Technology, Mekelweg 15, 2629 JB Delft, The Netherlands

E-mail: p.dorenbos@tudelft.nl

Received 21 December 2008, in final form 17 March 2009
Published 18 May 2009
Online at stacks.iop.org/JPhysCM/21/235605

Abstract

The scintillation yield, scintillation decay, and x-ray excited emission of pure $LaCl_3$ was studied as a function of temperature between 80 and 600 K. Two broad band emissions centered around 325 nm and 400 nm were identified and correlated to emissions from two localized exciton states named STE_1 and STE_2, respectively. Different temperature dependences were observed for the short and long wavelength band intensity. From 80 to 150 K, the 400 nm band intensity increases at the expense of the 325 nm band intensity. Above 150 K almost all emission is in the 400 nm band. From 150 to 600 K, the intensity of this band decreases and its lifetime shortens. These results are analyzed and interpreted with a model that comprises the creation of STE_1 and STE_2 self-trapped excitons, thermally activated quenching of STE_1 and STE_2 emission, and thermally activated transfer of excitation energy from STE_1 to STE_2.

1. Introduction

The discovery [1–3] of the excellent scintillation properties of Ce^{3+} doped $LaCl_3$ and $LaBr_3$ around the year 2000 has led to many new research activities in the field of gamma-ray detectors. New detection instruments based on mainly $LaBr_3$:Ce are presently being developed for medical diagnostics [4], space exploration [5], homeland security [6], and other applications.

Besides applications, it is of considerable interest to improve understanding of the mechanism responsible for the excellent scintillation properties of the lanthanum halides. In [1, 7–9] we presented our first ideas on the scintillation mechanism in those compounds, and in [10] we presented new data and proposed a more elaborate mechanism for cerium doped $LaBr_3$. It comprises Ce excitation by prompt trapping of free charge carriers and delayed excitation of Ce by means of a thermally activated transport of self-trapped excitons (STEs). Examples were given to demonstrate how those transport processes influence the $LaBr_3$ scintillation response. A major conclusion was that $LaBr_3$ scintillation characteristics are highly governed by the properties of the STEs created during gamma-ray excitation of the sample. At low Ce concentration (≈0.1%) and low temperature (≈100 K), STEs are created with high efficiency. Thermally activated STE diffusion to Ce is then the dominant scintillation mechanism. It results in relatively slow scintillation decay components (100 to >1000 ns). If the Ce concentration or the temperature increases, the speed of STE energy transfer to Ce increases. At high Ce concentration or high temperature, the transfer rate from STEs to Ce is faster than the lifetime (15 ns) of the 5d excited state of Ce. The scintillation decay profile is then entirely governed by that lifetime. For intermediate cerium concentrations and temperatures, all these mechanisms are present simultaneously and slow and fast components are mixed.

In addition to an experimental and qualitative description of the $LaBr_3$:Ce scintillation mechanism, we extended our research in order to quantify the role of the STEs in the $LaBr_3$:Ce scintillation process. We presented a mathematical relationship between the scintillation process and the role of STEs. A set of kinetics equations, solved numerically, was successfully applied to describe the temperature dependence of gamma-ray excited scintillation decay curves and light output as a function of cerium concentration [10]. A fit of this model combined with experimental data provided detailed information on the energy transfer between STEs and cerium ions as a function of cerium concentration and temperature.

Considering the similarities between the scintillation properties of $LaCl_3$:Ce and $LaBr_3$:Ce we expect that their scintillation mechanisms are also similar. To strengthen and to refine our model, more data are needed on the scintillation

properties of the undoped lanthanum halide compounds. First studies on undoped $LaCl_3$ were reported in [7, 9]. In this paper, we further investigated the scintillation properties of pure $LaCl_3$. Temperature dependence of x-ray excited emission, γ-ray scintillation light yield, and γ-ray scintillation decay times are presented and analyzed in terms of the creation of two types of self-trapped excitons called STE_1 and STE_2. The thermally activated quenching of STE_1 and STE_2 emission, and either the thermally activated transfer of excitation energy from STE_1 to STE_2 or the transformation from STE_1 into STE_2 appear to play an important role in the scintillation mechanism.

2. Experimental details

For this study we used pure $LaCl_3$ crystals with sizes ranging from 0.1 to 0.5 cm^3. An x-ray tube with Cu anode operating at 40 kV and 25 mA was used to generate x-ray excited luminescence. The spectra were recorded with an ARC VM504 monochromator (blazed at 300 nm, 1200 grooves mm^{-1}) and a Hamamatsu R323 photomultiplier tube with cathode potential of −1000 V. The spectra were corrected for the wavelength dependence of the photodetector quantum efficiency as well as for the monochromator transmission. X-ray excited luminescence measurements were performed between 100 and 600 K using a Janis liquid nitrogen bath cryostat.

We constructed a set-up to record scintillation pulse height spectra and scintillation decay time spectra upon ^{137}Cs (7.4 MBq) gamma-ray excitation as a function of temperature [11]. A sample was fixed at the bottom of a parabolic-like stainless steel cup that was mounted onto the cold finger of a liquid nitrogen bath cryostat. The cup directed the scintillation light through a window towards a photomultiplier tube (PMT) situated outside the cryostat. That PMT (XP2020Q at −2300 V bias) remained at room temperature and observed nearly all emitted scintillation light. For the pulse height measurements, its output was integrated via a home-made preamplifier and shaped by a spectroscopic amplifier (Ortec 572). These measurements provide us with the relative scintillation yield as a function of temperature. The absolute yield in photons per mega electronvolt absorbed gamma-ray energy (ph MeV^{-1}) at room temperature was obtained by the same technique as outlined in [12]. For recording decay curves covering four orders of magnitude in scintillation intensity the traditional start–stop method was used. The same PMT as used for pulse height recording now acted as the Start PMT. The Stop PMT (XP 2020Q at −2400 V) was mounted at the opposite side of the sample holder. Via a window and a small hole drilled through the cold finger and the bottom of the reflecting cup, single photons from the scintillation events were observed. The electronic part of the set-up was identical to the conventional delayed-coincidence method. LeCroy 934 constant fraction discriminators (CFDs) and a LeCroy 4208 time to analog converter (TAC) were used.

$LaCl_3$ is very sensitive to moistening even under vacuum conditions. For the room temperature measurement, the experiments were performed inside a dry box with a moisture content less than 1 part per million. For the temperature dependent measurements, the vacuum chamber and the cryostat without sample were baked at 400 K for two days. During the baking process all the water was removed from the experimental set-up. The pressure was less than 10^{-7} mbar. The sample chamber with cryostat was then vented inside the dry box and inside the dry box the sample was mounted onto the cold finger of the cryostat.

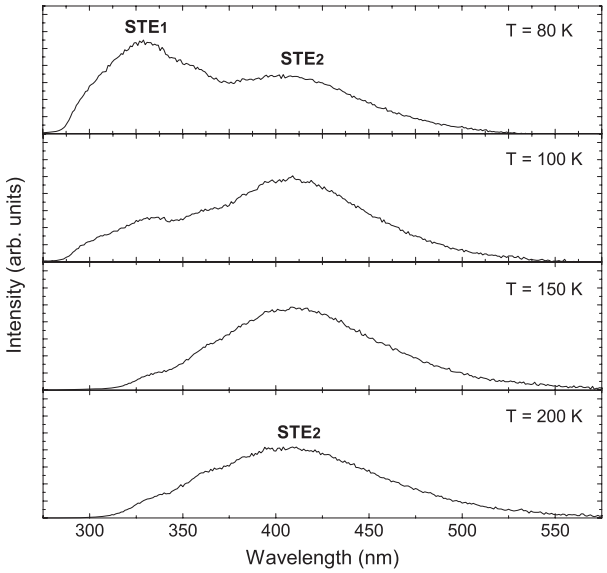

Figure 1. Temperature dependence of x-ray excited emission spectra of pure $LaCl_3$ recorded at 80, 100, 150, and 200 K.

3. Scintillation properties

In this section, we first present x-ray excited emission spectra that reveal two characteristic broad band emissions which we later will identify as due to STEs. Spectra recorded as a function of temperature reveal an anti-correlation between these two STE emission intensities. Next, gamma-ray excited scintillation light yield is determined as a function of temperature. The absolute light yield turns out to be consistent with the integrated x-ray emission intensity. Finally, the gamma-ray scintillation decay profiles are presented as a function of temperature.

3.1. X-ray excited emission spectra

Figure 1 shows the temperature dependence of x-ray excited emission for pure $LaCl_3$ at 80, 100, 150, and 200 K. Two broad emission bands are present. The one at 400 nm is attributed to STE emission and will be denoted as the low energy STE_2 band. It has been observed before and is also present in Ce^{3+} doped $LaCl_3$ [1, 7, 9]. In figure 1 we observe a second broad emission band peaking at 325 nm which will be referred to as the high energy STE_1 band. At 80 K, the emission is dominated by this high energy band. With increasing temperature, the low energy band emission increases at the expense of the high band emission. Above 150 K, almost all emission is in the low energy band.

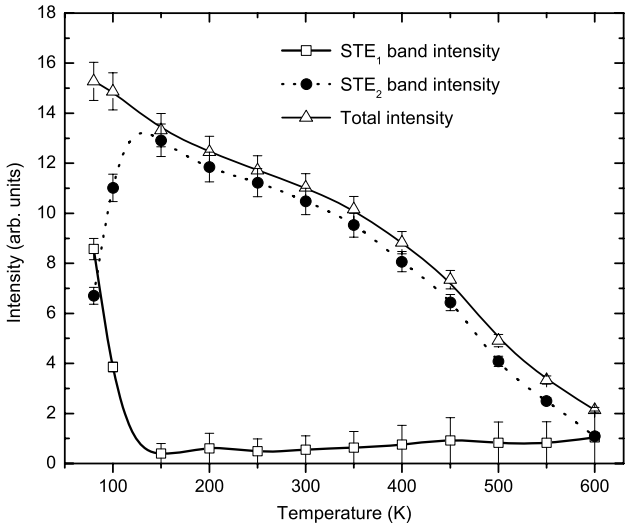

Figure 2. Temperature dependence of the light yields of high energy band STE_1, low energy band STE_2, and total luminescence in pure $LaCl_3$, derived from x-ray excited emission spectra. Curves are drawn to guide the eye.

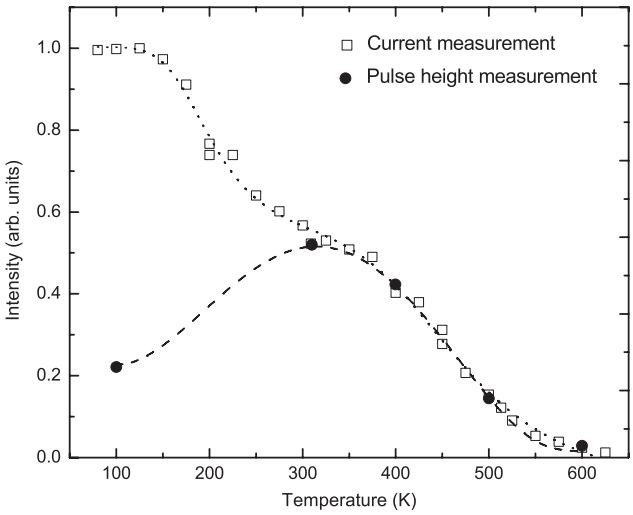

Figure 3. Temperature dependence of pure $LaCl_3$ scintillation yield obtained from ^{137}Cs source pulse height measurements (solid circles) or from the PMT anode current (open squares). Dashed lines are drawn to guide the eye.

These results resemble the results for pure $LaBr_3$. In $LaBr_3$, excitation in the 244 nm exciton absorption band yields at 10 K two broad band emissions at 330 m and 440 nm [13]. With temperature increase the intensity of the 440 nm increases at the expense of the 330 nm intensity, and at 150 K only the 440 nm band remains.

By fitting the emission spectra of pure $LaCl_3$ as a function of photon energy with two Gaussian-shaped bands, the integral intensities of the two STE bands were determined. Figure 2 shows the temperature dependence between 80 and 600 K of the high energy band intensity, the low energy band intensity, and the total luminescence intensity.

With increasing temperature, the total luminescence intensity decreases. An initial photon loss of about 15% is visible between 80 and 150 K. Above 150 K the curve shows a smaller slope. At 600 K, the photon loss corresponds to 85% of the light output measured at 80 K. As the temperature increases from 80 to 150 K, the low energy band luminescence intensity increases at the expense of the high energy band luminescence intensity. Above 150 K, the temperature dependence of STE_2 intensity is similar to that of the total intensity.

3.2. Scintillation yield

Figure 3 shows the relative scintillation yield of pure $LaCl_3$ at five different temperatures obtained from gamma-ray pulse height measurements with a shaping time of 10 μs. A separate determination of the absolute scintillation yield at room temperature with 10 μs shaping time gave $\approx$35 000 ph MeV^{-1}. By recording the PMT anode current as a function of temperature during γ-ray excitation of the crystal we can also obtain the relative scintillation yield as a function of temperature. Those results are also shown in figure 3. All three types of experiments were performed under ^{137}Cs 662 keV γ-ray excitation

For the current measurements, the maximum intensity is reached at 80 K. The dotted curve through the data shows a double bump shape. A first plateau from 80 to 125 K is followed by a 50% decrease of yield ending in a second plateau from 300 to 350 K which is followed by the remaining 50% decrease. Above 300 K, the relative yields obtained from the pulse height measurements follow a similar curve as that from the PMT anode current measurements. However, at 100 K the yield obtained from the pulse height measurement is almost five times smaller. This is attributed to the so-called ballistic deficit. As will be shown later, below 300 K a large part of the scintillation pulse becomes slower than the electronic shaping time of the preamplifier and shaping amplifier. That part of the scintillation pulse then does not contribute to the pulse height output of the shaping amplifier but it still contributes to the recorded PMT anode current. Above 300 K the scintillation response is significantly faster than the electronic shaping time.

Comparing the temperature dependence of the gamma-ray scintillation yield by means of the PMT anode current with that obtained from x-ray excited emission spectra we observe a similar behavior above room temperature. Below room temperature the anode current yield data appear to increase more than the x-ray excited luminescence yield. Actually a fair comparison cannot be made because the spectral profile of emission changes with temperature and the data from the PMT anode current measurements were not corrected for that. Furthermore, both emission profile and scintillation yield are not necessarily the same for low energy x-rays and high energy gamma-rays. Nevertheless, the general appearance of the curve from x-ray emission data is similar to that from the PMT anode current measurements.

The energy required to create one free electron and one free hole in an insulating compound is about 2.5 times the mobility band edge energy of that compound [14, 15]. Then with a mobility band gap of about 7.0 eV for $LaCl_3$ we anticipate 57 000 ionization MeV^{-1} of absorbed energy.

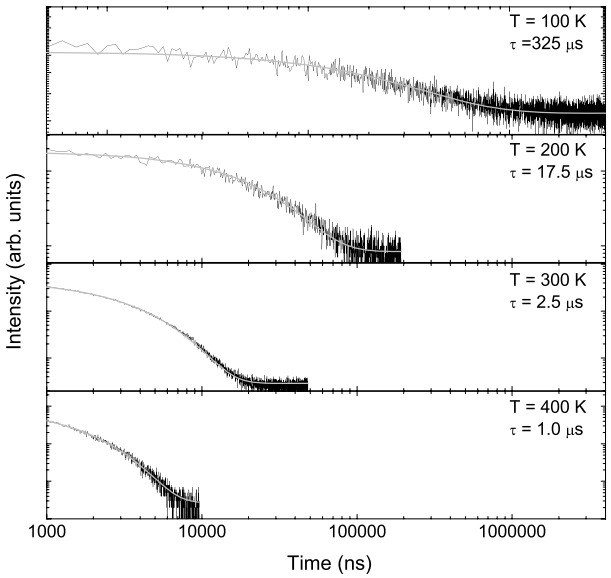

Figure 4. Temperature dependence of STE_2 (see text) scintillation time profiles in pure $LaCl_3$ in a log–log scale representation. The solid curve represents the fitted exponential decay function.

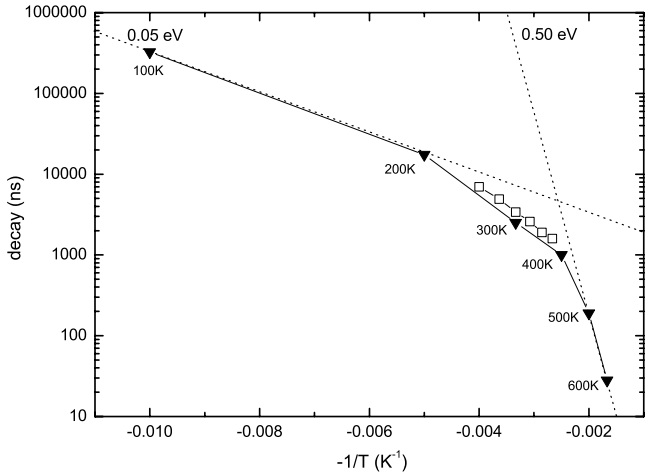

Figure 5. Temperature dependence of STE_2 (see text) scintillation lifetime in pure $LaCl_3$. The solid line is drawn to guide the eye. The open square data symbols are from data in [9]. The two dashed lines represent Arrhenius behavior with activation energies of 0.05 and 0.50 eV.

Table 1. Results from fitting the STE_2 scintillation decay profile of pure $LaCl_3$ as a function of temperature.

Temperature (K)	τ (ns)
100	325 000
200	17 500
300	2 500
400	1 010
500	192
600	28

With a measured absolute yield of about 35 000 ph MeV^{-1} at room temperature, figure 2 predicts a yield of about 50 000 ph MeV^{-1} and figure 3 of about 67 000 ph MeV^{-1} at temperatures below 100 K. Both are reasonably close to the predicted number of ionizations, and this indicates that at temperatures below 100 K each ionization creates one STE that decays radiatively with almost 100% quantum efficiency. Note that for the absolute yield of $LaCl_3$:10%Ce^{3+} we found 49 000 ± 3000 ph MeV^{-1} [12].

3.3. Scintillation time profiles

Figure 4 shows the temperature dependence of gamma-ray excited STE_2 scintillation time response for pure $LaCl_3$ at 100, 200, 300, and 400 K. The emission was selected with a broad band filter (400–600 nm). The time response is presented in a log–log representation. The decay is strongly temperature dependent and shows one exponential decay component. Figure 5 and table 1 show the decay time constants extracted from single exponential fits. The data are displayed in an Arrhenius representation as $^{10}\log(\tau)$ against the inverse temperature. For comparison, data from [9] are also shown and these are in good agreement with our own data. Note, that at 200 and 100 K the decay time is 1.7 and 32 times longer than the shaping time of 10 μs used for the pulse height measurements in figure 3.

4. Scintillation model: discussion

To analyze the data and to translate it into a scintillation mechanism for pure $LaCl_3$, we will proceed in three steps. We first discuss phenomenologically the mechanism responsible for the observed scintillation properties. Next a mathematical model based on a set of rate equations is formulated and used to reproduce the temperature dependence of the intensity of the two STE emissions observed in x-ray excited emission spectra. This approach will validate our hypothesis. Finally, we will relate the model to the defect properties and mobility of charge carriers and excitons in $LaCl_3$ on an atomic level.

4.1. Phenomenological description and model hypothesis

We distinguish two main energy and charge carrier transfer processes in pure $LaCl_3$, i.e. the sequential capture of charge carriers by chloride ions leading to the creation of STE_1, and the thermally activated energy transfer from STE_1 to STE_2. In our model, STE_1 and STE_2 emissions are attributed to two different types of STEs. This attribution is mainly based on x-ray excited electron-paramagnetic-resonance spectra that reveal signatures of two types of STEs [16]. Furthermore the width of the emission bands are typical for STE-like emission. The two STE types correspond to two configurations of *out of plane* STEs formed by two nearest Cl^- neighbors [16].

Process I is the prompt capture, i.e. faster than 1 ns, of a free hole (h^+) and a free electron (e^-) from the ionization track by two chloride ions, leading to the creation of STE_1 and followed by STE_1 emission. This emission corresponds to the broad band emission centered at 325 nm in figure 1.

$$2Cl^- + h^+ \rightarrow V_k \quad (1)$$

$$V_k + e^- \rightarrow STE_1 \quad (2)$$

$$STE_1 \rightarrow \nu\,(325\ \text{nm}). \quad (3)$$

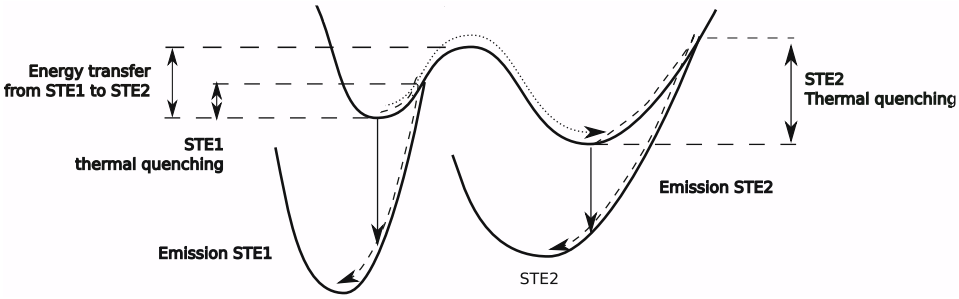

Figure 6. Scheme illustrating the scintillation mechanism in pure $LaCl_3$.

The emission of STE_1 may quench thermally which leads to a decrease of the total emission intensity between 80 and 150 K under x-ray excitation in figure 2, and between 150 and 250 K under gamma-ray excitation in figure 3. One may speculate that the lower thermal quenching temperature under x-ray excitation might be related to an on average higher density of ionizations, and consequently STE_1 concentration, created by the relatively low energy (10–30 keV) x-ray ionization tracks.

Process II is a thermally activated energy transfer from STE_1 to STE_2, leading to the broad band emission centered at 400 nm.

$$STE_1 \rightarrow STE_2 \tag{4}$$

$$STE_2 \rightarrow h\nu\,(400\ \text{nm}). \tag{5}$$

The transfer from STE_1 to STE_2 is revealed by the changing STE_1 and STE_2 emission intensities between 80 and 150 K in figures 1 and 2. The anti-correlation between STE_1 and STE_2 luminescence intensity shows that the energy located on STE_1 transfers to STE_2. The scintillation response due to STE_2 emission in figure 4 at times longer than 1 μs is described by a single exponential decay for all temperatures between 100 and 600 K.

Like STE_1, STE_2 emission is also thermally quenched. This quenching leads to the emission losses observed above 200 K under x-ray excitation in figure 2 and above 300 K under gamma-ray excitation in figure 3. Further evidence for thermal quenching of STE_2 emission is provided by the shortening of STE_2 emission decay observed above 300 K in figures 4 and 5. As expected for a thermal quenching mechanism, the temperature dependences of lifetime and yield follow the same trend.

The entire scintillation model is further illustrated in figure 6. It shows a double well curve with, on the left upper side, the excited state of STE_1 and, on the right upper side, the excited state of STE_2; separated from each other by a potential energy barrier. The height of that barrier represents the activation energy for thermally activated STE transport or transfer. The STE_1 and STE_2 ground states are represented by two separate parabolas that both intersect the double well curve. Thermal quenching of STE_1 and STE_2 emission proceeds via those intersection points.

4.2. Mathematical description

Using rate equations, the different processes of the scintillation mechanism can be described mathematically. We will focus on the events that follow the absorption of a single gamma-ray photon. The production of free electrons and free holes in the ionization track is assumed to be instantaneous, as are the sequential capture of free electrons and holes by chloride ions leading to the formation of STE_1s. This assumption is justified since the time resolution (more than 1 ns) of the experimental data to which our model will be applied is longer than the STE creation time.

The processes in pure $LaCl_3$ can be described mathematically by the following rate equations:

$$\frac{dn_{STE_1}}{dt} = -\Gamma_{STE_1} n_{STE_1} - \Gamma_T n_{STE_1} - \Gamma_{Q_1} n_{STE_1} \tag{6}$$

$$\frac{dn_{STE_2}}{dt} = -\Gamma_{STE_2} n_{STE_2} + \Gamma_T n_{STE_1} - \Gamma_{Q_2} n_{STE_2} \tag{7}$$

where n_{STE_1} and n_{STE_2} are the number of STE_1 and STE_2 in the crystal. Γ_T is the transfer rate from STE_1 to STE_2. Γ_{STE_1} and Γ_{STE_2} are the radiative decay rates of STE_1 and STE_2. Γ_{Q_1} and Γ_{Q_2} are the STE_1 and STE_2 non-radiative quenching rates. All three rates are assumed to follow an Arrhenius behavior, $\Gamma = \nu e^{(-E/kT)}$ with ν the frequency factor in s^{-1} and E the energy barrier in eV. The initial conditions are the numbers of STE_1s and STE_2s created at $t = 0$. In our model $n_{STE_1}(0) =$ 57 000 which corresponds to the number of electron/hole pairs per MeV created under gamma-ray excitation in pure $LaCl_3$ and $n_{STE_2}(0) = 0$.

The parameters $\Gamma_{Q_1} = \nu_{Q1} e^{(-E_{Q1}/kT)}$, $\Gamma_{Q_2} = \nu_{Q1} e^{(-E_{Q2}/kT)}$, and $\Gamma_T = \nu_T e^{(-E_T/kT)}$ are evaluated via a numerical integration of the rate equations and a least squares fitting process. The input file includes all the parameters from equations (6) and (7) together with the experimental data on the temperature dependence of the relative light output under x-ray excitation in figure 2. The output data reproduce the predicted light output as a function of temperature together with values for the parameters of the model. In figure 7, we have plotted for each temperature the experimental data as solid data symbols together with the result from a fitting process (gray curve). Table 2 presents the parameter values obtained from that fitting process. We have to note here that other sets of quenching and energy transfer parameters were also able to reproduce the main trends in the scintillation light output. Apparently there is

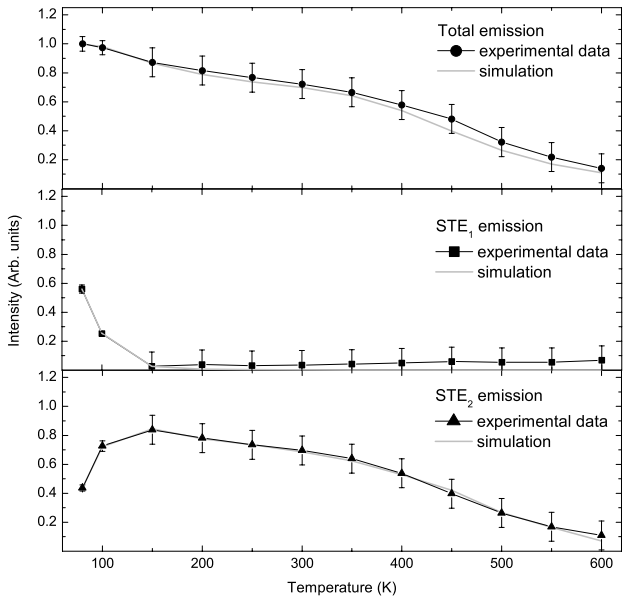

Figure 7. Temperature dependence of pure $LaCl_3$ scintillation yield derived from x-ray excited emission spectra and from our model simulation.

not a deep and unique minimum in the parameter configuration space. Possibly this is related to an oversimplification of our model and the assumption that all three rates follow Arrhenius behavior.

Our model reproduces the main characteristics of the STE_1 and STE_2 x-ray excited emission intensities as a function of temperature. The fit of the experimental data over the entire temperature range provides support for our model and its hypothesis that the scintillation light output of pure $LaCl_3$ results from the competition of three different processes: the thermal quenching of STE_1 and STE_2 intensities responsible for the photon emission loss in the material, and a thermally activated transfer from STE_1 to STE_2.

4.3. Discussion

From the experimental results presented in this paper, we propose a scintillation model for pure $LaCl_3$. The model allows us to further discuss the microscopic mechanisms responsible for the observed thermally activated processes.

As suggested by figure 2 and reproduced by the simulation, the primary charge carriers in the ionization track are captured by chlorine anions to exclusively form the STE_1 type of STEs. At 80 K about 40% of STE_1 transfers its energy to STE_2, as shown in figure 1. The remaining part decays radiatively, creating the STE_1 emission band. At 150 K there is 15% loss in total emission intensity which must be attributed to non-radiative decay of STE_1. The other 85% of the STE_1s transfer their energy to STE_2. STE_1 emission is absent at 150 K. Clearly $\Gamma_T > \Gamma_{Q_1} > \Gamma_{STE_1}$. When temperature increases from 150 to 300 K we see a further loss in the total emission by about 15%. If non-radiative decay of STE_2 emission is not yet significant then the loss must be attributed to quenching of STE_1 before it transfers to STE_2. It would

Table 2. Activation energies and frequency factors obtained from a least squares fitting of our model to the temperature dependent x-ray excited emission intensities of STE_1 and STE_2 emission in pure $LaCl_3$.

E_{Q1} (eV)	ν_{Q1} (s^{-1})	E_{Q2} (eV)	ν_{Q2} (s^{-1})	E_T (eV)	ν_T (s^{-1})
0.08	10^8	0.34	10^{10}	0.11	10^{10}

imply that although below 150 K $\Gamma_T > \Gamma_{Q_1}$, Γ_{Q_1} increases more rapidly with temperature than Γ_T, or $E_{Q1} > E_T$. Another possibility is that non-radiative decay of STE_2s does take place below 300 K. Finally above 300 K, the loss in total emission intensity must be attributed to non-radiative decay of STE_2s. Intensity loss with increasing temperature goes along with decay time shortening, see figure 5.

At temperatures above 100 K, equations (6) and (7) reduce to:

$$\frac{dn_{STE_1}}{dt} = -(\Gamma_T + \Gamma_{Q_1})n_{STE_1} \tag{8}$$

$$\frac{dn_{STE_2}}{dt} = -\Gamma_{STE_2}n_{STE_2} + \Gamma_T n_{STE_1} - \Gamma_{Q_2}n_{STE_2}. \tag{9}$$

Solving equations (8) and (9) gives n_{STE1} and n_{STE2} as a function of time:

$$n_{STE_1}(t) = n_{STE_1}(0)e^{-(\Gamma_T+\Gamma_{Q_1})t} \tag{10}$$

$$n_{STE_2}(t) = \frac{n_{STE_1}(0)}{(\Gamma_T + \Gamma_{Q_1})}e^{-(\Gamma_T+\Gamma_{Q_1})t}(e^{-(\Gamma_{STE_2}+\Gamma_{Q_2}-\Gamma_T)t} - 1). \tag{11}$$

If Γ_{STE_2} is much smaller than $(\Gamma_T + \Gamma_{Q_1})$, all the transfer has taken place already before the STE_2 starts to decay. STE_2 decay is determined by Γ_{STE_2} only. This process applies at temperatures above 300 K. Then the thermal quenching of STE_2 emission expressed by Γ_{Q2} is responsible for the shortening of STE_2 lifetime in figures 4 and 5, and of the photon emission loss in figure 3. If Γ_{STE_2} is of comparable magnitude to $(\Gamma_T + \Gamma_{Q_1})$, say, from ten times slower to ten times faster, then STE_2 lifetime is determined by the competition between the transfer rate from STE_1 to STE_2 and the sum of the radiative, Γ_{STE_2} and non-radiative, Γ_{Q_2} rates. This process is visible between 100 and 300 K in figures 4, 5, and 3. When the temperature increases, Γ_T becomes faster leading to a shortening of STE_2 lifetime. Note that equation (11) predicts a rise time in the scintillation pulse that is controlled by the value for $\Gamma_T + \Gamma_{Q1}$. In the time range of our measurements of figure 4 we did not observe such a rise time, and apparently the rise is much less than 1 μs.

Apart from the studies in [16] we do not have detailed information on the true nature of the STE_1 and STE_2 defects. However, the present work did reveal that the STE_1 defect can transform into the STE_2 defect. We envisage two possibilities: (1) STE_1 and STE_2 are two excitons at spatially uncorrelated sites, and the activation energy for the transfer could be due to a thermal activated process for STE_1 to jump from one crystallographic site to the other. (2) STE_1 and STE_2 are two different types of excitons that can exist at the same site in the lattice. The activation energy is the energy barrier to simply transform STE_1 into the structural configuration corresponding with STE_2.

5. Conclusion

X-ray excited emission spectra, gamma-ray pulse height spectra, and scintillation decay time profiles were measured between 80 and 600 K on pure $LaCl_3$. The results were analyzed with a scintillation model that contains the following energy and charge carrier transfer and quenching processes.

- The prompt sequential capture of the primary charge carriers by two chloride ions to form a self-trapped exciton (STE_1).
- A thermally activated process that transfers STE_1 into another self-trapped exciton STE_2.
- A thermal quenching mechanisms for STE_1 and for STE_2 luminescence.

The competition between all those processes determines the scintillation properties as a function of the temperature. At temperatures below 150 K, STE_1 is the main emitting center present in pure $LaCl_3$. Photon losses are due to the thermal quenching of STE_1 emission. When the temperature increases, STE_1 disappears and STE_2 is created. It results in an additional photon loss mechanism due to the thermal quenching of STE_2 emission. Above 300 K, the scintillation properties are entirely governed by the intrinsic properties of STE_2. For intermediate temperatures, all these mechanisms are present simultaneously and the scintillation properties of pure $LaCl_3$ are the result of the competition between those different thermally activated processes. By means of a set of rate equations based on these models a qualitative agreement with the available data was obtained.

Acknowledgments

This work was financed by the Idaho National Engineering and Environmental Laboratory and the USA Department of Energy. We thank the company Saint Gobain, division crystals and detectors, Nemours, France for providing the scintillators used in this work.

References

[1] Guillot-Noël O, Dorenbos P, van Eijk C W E, Krämer K and Güdel H U 1999 *J. Lumin.* **85** 21
[2] van Loef E V D, Dorenbos P, van Eijk C W E, Krämer K and Güdel H U 2000 *Appl. Phys. Lett.* **77** 1467–8
[3] van Loef E V D, Dorenbos P, van Eijk C W E, Krämer K and Güdel H U 2001 *Appl. Phys. Lett.* **79** 1573–5
[4] Kuhn A, Surti S, Karp J S, Muehllehner G, Newcomer F M and VanBerg R 2006 *IEEE Trans. Nucl. Sci.* **53** 1090
[5] Kraft S, Maddox E, Buis E-J, Owens A, Quarati F G A, Dorenbos P, Drozdowski W, Bos A J J, de Haas J T M, Brouwer H, Dathy C, Ouspenski V, Brandenburg S and Ostendorf R 2007 *IEEE Trans. Nucl. Sci.* **54** 873–8
[6] Ayaz-Maierhafer B and DeVol T A 2007 *Nucl. Instrum. Methods* A **579** 410
[7] van Loef E V D, Dorenbos P, van Eijk C W E, Krämer K and Güdel H U 2001 *IEEE Trans. Nucl. Sci.* **48** 341
[8] van Loef E V D, Dorenbos P, van Eijk C W E, Krämer K W and Güdel H U 2002 *Nucl. Instrum. Methods* A **486** 254–8
[9] van Loef E V D, Dorenbos P and van Eijk C W E 2003 *J. Phys.: Condens. Matter* **15** 1367–75
[10] Bizarri G and Dorenbos P 2006 *Phys. Rev.* B **53** 615
[11] Bizarri G, de Haas J T M, Dorenbos P and van Eijk C W E 2006 *Phys. Status Solidi* a **203** R41
[12] de Haas J T M and Dorenbos P 2008 *IEEE Trans. Nucl. Sci.* **55** 1086–92
[13] Dorenbos P, van Loef E V D, Vink A P, van der Kolk E, van Eijk C W E, Krämer K W, Güdel H U, Higgins W M and Shah K 2006 *J. Lumin.* **117** 147
[14] Robbins D J 1980 *J. Electrochem. Soc.* **127** 2694
[15] Dorenbos P 2002 *Nucl. Instrum. Methods* A **486** 208–13
[16] Rogulis U, Schweizer S, Spaeth J M, van Loef E V D, Dorenbos P, van Eijk C W E, Krämer K W and Güdel H U 2002 *Radiat. Eff. Defects Solids* **157** 951